Asociación Argentina
de Mecánica Computacional

Mecánica Computacional Vol XXVII, págs. 181-205 (artículo completo)
Alberto Cardona, Mario Storti, Carlos Zuppa. (Eds.)
San Luis, Argentina, 10-13 Noviembre 2008

NUMERICAL AND EXPERIMENTAL IN-CYLINDER FLOW STUDY IN A 4-VALVE SPARK IGNITION ENGINE

Damian E. Ramajo and Norberto M. Nigro

International Center for Computational Methods in Engineering (CIMEC)
INTEC-Universidad Nacional del Litoral-CONICET, Güemes 3450
S3000GLN Santa Fe, Argentina
e-mail: dramajo@santafe-conicet.gov.ar, web page: http://venus.ceride.gov.ar/

Keywords: cold and hot dynamic and static engine simulation, Computational Fluid Dynamics (CFD), in-cylinder flow patterns.

Abstract. Numerical and experimental techniques were applied in order to study the in-cylinder flow field in a commercial 4-valve spark ignition engine Fiat Torque. Investigation was focused in analyze the generation and evolution of tumble-vortex structures during the intake and compression strokes, and the capacity of this engine to promotes the turbulence enhancement during tumble-vortex degradation, at the end of the compression stroke. For these purposes, three different approaches were developed. Firstly, static flow bench tests were experimentally carried out, and these were reproduced by computational fluid dynamics (CFD) simulations. Once the numerical techniques were assessed, a dynamic simulation of the full engine cycle was performed for several engine speeds (1500 rpm, 3000 rpm and 4500 rpm) without consider the combustion (cold dynamic simulation). Static and dynamic cold-engine results were compared in order to conclude about the significance of static-flow-test results to analyze the in-cylinder flow behavior.

Finally, combustion was taken into account and the full-cycle engine simulation (hot dynamic simulation) was developed for the same three engine speeds. Combustion phenomenon was introduced as an in-cylinder homogeneous heat source. For this, a simple predicting model was proposed in order to estimate the combustion rate as a function of the mean in-cylinder flow conditions (temperature, pressure, turbulent intensity and geometry of the combustion chamber). In addition, to getting more realistic results, 0/1-dimensional simulations were performed in order to feed appropriate boundary conditions for CFD simulations. All these results were employed to characterize the in-cylinder flow field of the engine, and at the same time, to conclude about the validity and usefulness of the different engine tests (static flow tests, cold dynamic and hot dynamic simulation) to estimate the mean-flow characteristics of the engine.

1. INTRODUCTION

In-cylinder charge motion is getting more and more importance since the introduction of new technologies like gasoline direct injection (GDI) or homogeneous charge compression ignition (HCCI). Understanding the behavior of the in-cylinder flow structures is the first step to control efficiently the fuel stratification, the turbulence generation and the heat losses. All these factors play a crucial role on fuel economy, emissions and of course engine performance.

For years, engine development has been mainly support by experimental techniques like dynamometric and static flow tests. Recently, the evolution of optical techniques allows to see inside the cylinder by using complex instruments and engines adapted to have optical access. But this kind of tests demands too much time and money. Besides, they are limited to low engine speeds and do not allow to analyze the whole combustion chamber at the same time. On the other hand, static flow bench tests are faster and cheaper but obviously give limited information about the engine behavior in real conditions and none about the flow patterns.

Until a few years ago, the study of engines by computational techniques was limited to use of 0/1-dimensional engine simulators, solving the cylinders by means of the application of mass and energy balances. Although these simulators are still massively employed for studying the gas dynamic of the overall engine configuration, in-cylinder processes are getting more relevance due to the necessity of improving the combustion stage and reducing emissions. For these reasons, computational fluid dynamics (CFD) is being progressively accepted as a useful tool to design complex engine parts like combustion chambers, manifolds or injectors. During the last years CFD techniques have been significantly improved, especially thanks to High Performance Computing (HPC), leading to researchers to introduce more realism in their simulations.

Nowadays the efforts are focused in obtaining in-cylinder simulations introducing injection of fuel, combustion and chemical species evolution for emission control. Nevertheless, although CFD is beating experience and credibility, experimental techniques like static bench and cold dynamic optical tests are daily employed.

In this work both experimental flow tests and numerical simulations were carried out in order to assess CFD estimations and understand the in-cylinder flow. Then CFD was applied to solve the in-cylinder flow behavior under dynamic conditions (moving the piston and valves) and results were related to those statically obtained in order to conclude about the usefulness of static flow tests.

2. METHODOLOGY

In this section the main characteristics of numerical and experimental static tests along with the numerical dynamic ones are presented. Due to the static test configurations are not standardized, it is important to define how each one of the different tests were performed. As regard the simulation of static tests, they were achieved reproducing as exactly as possible the experimental conditions.

In this work a commercial 4-valve Fiat Torque engine was employed. In table 1 are consigned the main constructive and operative characteristics of the engine.

Cylinder	
Fuel	Gasoline
Number of cylinders	4
Piston displacement	395.5 cm^3
Bore	87 mm
Stroke	68 mm
Compression ratio	10.5:1
Connecting rod length	118 mm

Valves configuration		
	Intake	Exhaust
Maximum lift	9 mm	8.5 mm
Diameter	30.4 mm	29.9 mm
Maximum lift CA	102.5º	618.5º
Opening range	255º	253º
Opening advance	25º	48º
Closing retard	50º	25º

Table 1: Constructive and operative characteristics of the engine (CA means Crank angle).

2.1 Experimental procedure. Static tests

Three kind of static tests were achieved; the flow-meter, the swirl and the tumble tests. For all cases, the cylinder head was subject to a constant pressure drop of 25 inch of water, using a flowmeter SuperFlow SF-600. A swirl meter (MS) with rotary honey comb was employed to perform the angular momentum measurements.

As regard discharge-coefficient tests both intake and exhaust systems were studied. Flow circulation was the naturally induced for the engine. That means that the flow was entering toward the cylinder for characterization of the intake system, while it was outgoing for the exhaust one. In order to reduce flow turbulence and acoustic effects, a 100 mm long cylinder was added below the cylinder head and a nozzle and a diffuser were put at the beginning and at the end of the intake and exhaust ducts, respectively. Seven valve lifts were considered for each analysis.

While the swirl tests were performed adding a swirl meter below (downstream) the 100 mm long cylinder, the tumble tests were done using an own designed system, an L-shape tumble bench configuration that was adopted in base of a CFD comparison with some of the main available bench configurations. Figure 1 shows a sketch of it. As can be seen, it has only one lateral duct to canalize the tumble vortex.

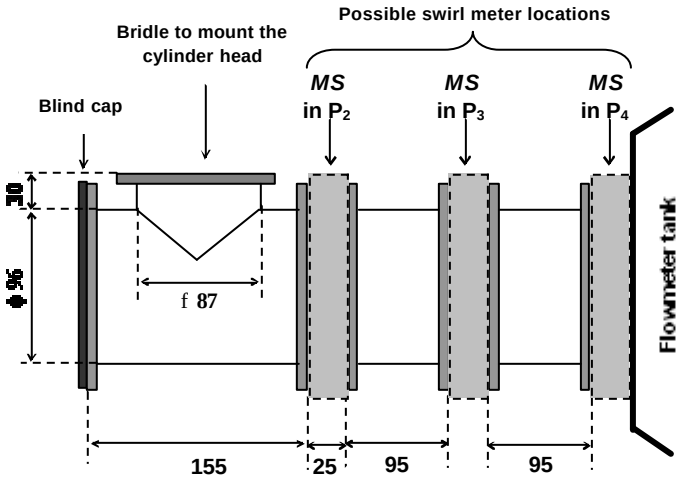

Figure 1: Sketch of the tumble bench configuration employed to perform the tumble tests.

The proposed tumble bench configuration has some interesting characteristics; firstly the angular momentum loss along the lateral duct is diminished because the lateral duct diameter is larger than the cylinder bore. Moreover, momentum loss is almost linear along the lateral duct. Secondly, the fact it has a unique lateral duct produces a more intense angular momentum over

the swirl meter. Thirdly, the local angular-momentum loss at the joint between the cylinder and the lateral duct is negligible, so in-cylinder tumble estimation can be done by linear extrapolation from two measures over the lateral duct. Finally, although L-shape configurations are not symmetric with respect to the cylinder mean plane, for this design there are not differences in the tumble momentum induced by any of both intake valves, that is, both valves produce the same tumble without take into account which one is closer to the lateral duct. It is explained by the height from the lateral duct to the bridle (30 mm) and the fact that the joint between the cylinder and the lateral duct is symmetric (Ramajo, 2008).

2.2 Numerical procedure

2.2.1 Construction and meshing of the computational geometry

In order to generate the engine geometry, positive replicas from the intake and exhaust ducts (using low-contraction silicone) and the combustion chamber (employing high rigid polyester resin) were performed. Figure 2 at left shows a picture of the three replicas, which were assembled by means of four steel sticks inserted through the valve guides. Afterwards, each replica was introduced inside a three dimensional rotary laser scanner (Roland LPX-250), obtaining a large amount of Cartesian coordinate points (around 550.000 points) over the replicas surface. Points were transferred to software GID 7.2 and some of them were selected in order to draw pathlines. Then, lines were exported to ANSYS-ICEM 10.0 and employed to build small patch surfaces, obtaining the overall shape of the model. Figure 2 at right shows the final computational domain.

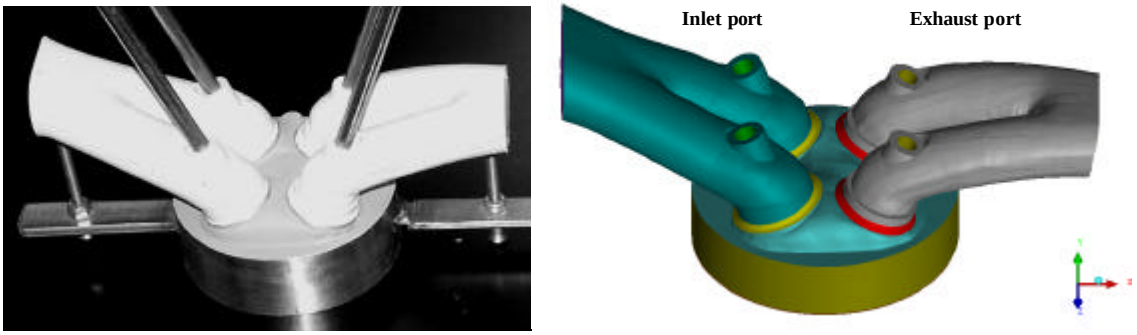

Figure 2: *Left:* positive replica of ports and combustion chamber of the engine. *Right:* model constructed based on laser measurement of replica.

Meshes were generated employing ANSYS-ICEM 10.0. Around 2×10^6 tetrahedral elements were required to get an accurate description of the static-test geometries, in particular around valves region. A mesh convergence study allowed us to define the optimum element size, resulting closer to 1.1 mm. CFD models were solved using a cluster Beowulf (aquiles-cluster, 2008) for distributed calculus. 20 nodes (processors single core) were employed to perform the simulations, spending around 24 hours to get each valve lift position in the static tests.

2.2.2 Static simulations

Static simulations were carried out reproducing the experimental test conditions. For flow tests, the cylinder head was subject to a constant pressure drop, which was progressively increased from 0 to 25 inch water, in order to avoid convergence problems. The intake and exhaust systems were studied obeying the naturally induced flow circulation of the engine. That

means flow was entering toward the cylinder for intake characterization while outgoing for the exhaust one.

Results were obtained by applying the Navier-Stokes balance equations for mass and momentum (isothermal model). Turbulence was modeled through a *k-e* standard model. Simulations were transients and a minimum of 1000 time steps were obtained for each case. Then the final results were obtained through a time averaged of 10 time steps over the simulated period. A suitable time step was obtained from a time-convergence study, resulting equal to $5x10^{-5}$ seconds for all cases.

A total pressure was fixed at inlet boundary while for the outlet boundary an opening condition was employed (it allows flow to leave from or enter to domain according the pressure differences at both sides of the boundary). A non slip condition was choice for walls and a roughness of 0.2 mm was applied to the ducts walls.

2.2.3 Dynamic simulations

Even though combustion was not considered in dynamic simulations, the energy balance equation was also solved in order to take into account the temperature increment due to the compression work.

Tackling the dynamic simulation of the whole engine cycle involves at least two complex problems; the mesh deformation and the topological changes of the geometry. The extreme displacement of piston and valves introduces large mesh deformations that can be solved by two ways; firstly, using an algorithm capable to move the mesh nodes without producing invalid meshes (meshes having collapsed elements with negative volume). Secondly, employing a combination of mesh deformation in each time step and remeshing after several time steps in order to preserve the mesh quality. In this research the second alternative was chosen and 17 remeshing were needed to complete the engine cycle. Mesh motion calculus was done by applying a laplacian equation to obtain the position of the internal nodes fom the imposed displacements of certain nodes (over the piston head and valves surfaces). As noted, the number of remeshing needed to complete the engine cycle is significant, involving a laborious work to perform the engine geometries. The mesh motion method incorporated in ANSYS-CFX is not robust enough to save remeshing and better algorithms, like the introduced by Lopez et al. (2008), can be used to reduce remeshing from 17 to only 4.

As for piston motion, it was employed the well known crank-slider mechanism expression (Heywood, 1988) while the valve lift vs. crankshaft angle law for intake and exhaust valves were obtained by measurements and introduced to the simulations through an external Fortran routine.

As regard topological changes, the engine cycle starts with the valve overlap and for the firsts 16 CA the intake and exhaust ducts are connected with the cylinder (domain *ICE* at figure 3). Then the exhaust valves are closed and the exhaust duct is separated from the cylinder. Intake process continues meanwhile the exhaust duct is simulated separately. 5 more remeshings are necessary to complete the *IC* domain simulation (from 16 to 208 CA). Once intake valves are closed (at 208 CA) three isolated domains have to be simulated (domains *I*, *C* and *E*). At 492 CA the exhaust-valve opening connects again the exhaust duct with the cylinder (domain *CE*) and the solutions from two isolated domains have to be loaded to the assembled domain *CE*. For this purpose a software call to a user defined external Fortran routine was included to feed the initial conditions for temperature, pressure and turbulence from data in domains *C* and *E*. The Fortran routine searches in the isolated mesh to find the element where is contained each node of the assembled mesh (using an algorithm of directed search (Ramajo, 2008), and then uses finite element interpolation to find the corresponding value. The same

strategy is employed for intake valve opening. As it was mentioned, the extreme deformations of the mesh around valve seats are one of the most difficult obstacles during the engine dynamic simulation. For this end, the minimum gap between valves and seats was limited to 0.8 mm. That is, domains connect or disconnect when valve lifts reaches 0.8 mm or less. Of course, this fact reduced the valve opening period, but the mass flow through valves for lifts below 0.8 mm can be scorned.

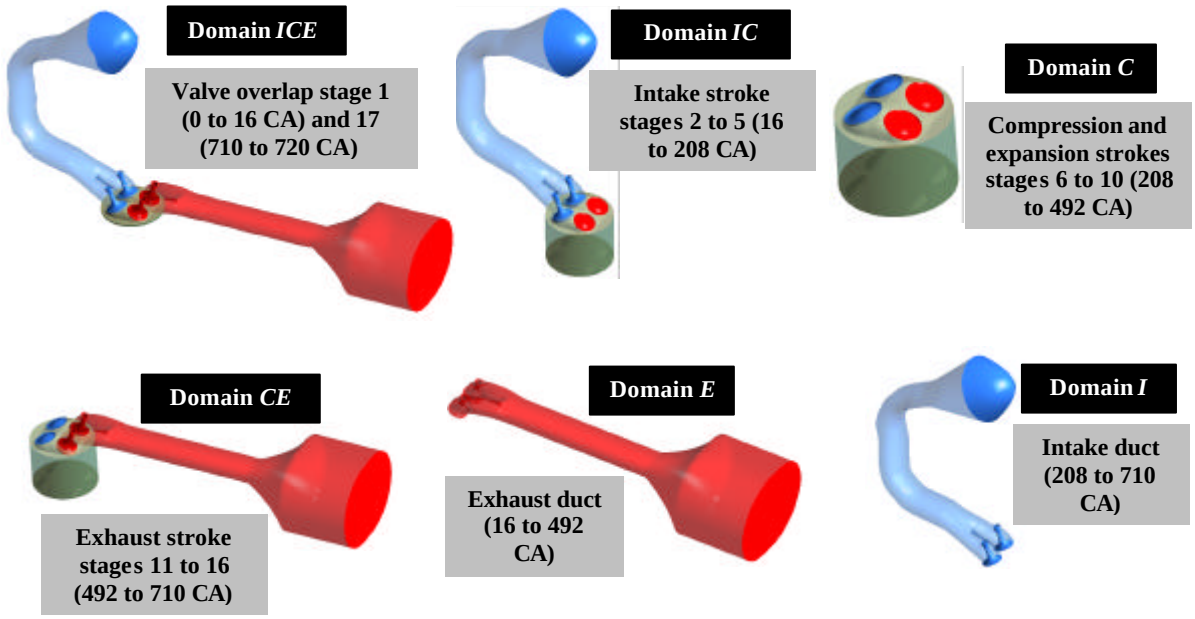

Figure 3: Different domains employed to simulate the whole engine cycle.

Although running several isolated domains is laborious, it allows use different time steps for the cylinder and ducts. Taking into account that gas velocity in isolated ducts is very low, the time step for them can be increased several times reducing computational time without introducing convergence problems.

The time step at 1500 rpm was $5x10^{-5}$ seconds (the same that was used for static simulations), but in order to keep the Courant number almost constant, it was reduced to $2.5x10^{-5}$ seconds and $1.66x10^{-5}$ seconds for 3000 rpm and 4500 rpm, respectively.

Regarding the computational resources, 10 cluster processors were employed, demanding approximately 40, 80 and 120 hours of cpu time to solve one thermodynamic cycle (0 CA to 720 CA) for 1500 rpm, 3000 rpm and 4500 rpm, respectively.

2.2.4 Combustion modeling

A very simple combustion model was implemented in order to quantify the influence over the in-cylinder flow characteristics due to the temperature and pressure increments caused by combustion. For spark-plug homogeneous charge engines, the combustion phenomena can be classified under the regimen knew as flamelet. In it, combustion takes place in a very thin zone (a few millimeters) were combustion is nearly laminar. Then, the flow has the effect of strengths and corrugates the thin zone, increasing the flame front surface area and enhancing the reactant mixing. The advantage of the flamelet combustion regimen is that flow and combustion evolution can be solved in a separated way, just introducing the combustion effect through a heat source in the energy balance equation (Williams, 1985; Tan and Reitz, 2006).

The combustion model was introduced through an External Fortran Routine, which takes same state variables like the in-cylinder averaged pressure and temperature and turbulence quantities (k and e), and estimates the turbulent burning velocity (S_t) of the flame under these conditions applying a model based on the fractal theory and the Kolmogorov hypothesis:

$$\frac{S_t}{S_l} = \frac{A_t}{A_l} \approx \left(\frac{l_e}{l_i}\right)^{D_3-2}, \tag{1}$$

being S_l the laminar propagation velocity of the flame, A_t and A_l the turbulent and laminar flame front areas, l_e and l_i the turbulent spatial scales of outer and inner cut (related with the size of the biggest turbulent structures and the smallest ones), and finally D_3 is the fractal dimension. The turbulent scales l_e and l_i was represented by the integral and the Kolmogorov scales, while for the fractal dimension the correlation gave for North and Santavicca (1990) was employed:

$$D_3 = C_1 \frac{u'}{u'+S_l} + C_2 \frac{S_l}{u'+S_l}. \tag{2}$$

In equation (2) u' is the turbulent intensity and C_1 and C_2 are model constants (C_1 = 2.35 and C_2 = 2.0). Returning to equation (1), in it the laminar burning velocity (S_l) must be estimated. For that, a well known correlation was introduced (Meghalchi and Keck, 1982):

$$S_l = S_{l0}\left(\frac{T_u}{T_0}\right)^a \left(\frac{p}{p_0}\right)^b (1-1.5Y_{res}), \tag{3}$$

being, S_{l0} a reference velocity (depending on fuel and stoichiometric relation), T_u the temperature of unburned gases and Y_{res} the fraction of residual gases. S_{l0} and constants α and β are obtained by:

$$S_{l0} = B_1 + B_2(\tilde{j} - j_0)^2,\ a = 2.18 - 0.8(\tilde{j} - 1) \text{ and } b = -0.16 + 0.22(\tilde{j} - 1). \tag{4}$$

Once the in-cylinder averaged turbulent burning velocity (S_t) has been obtained, it is performed a geometrical estimation of the front surface area by assuming that the flame front grows spherically (with the same S_t in all directions) from the spark plug position. The combustion model is not multi-zone. That is, there is a unique fluid and there is not a real interface representing the flame front. So, the flame front surface area estimation is only performed in order to calculates the fluid that would be burned by the hypothetic flame front growing with the velocity S_t. That allows to estimates the heat released in each time step, which is subsequently introduced to Navier-Stokes equations as a heat source. The heat source has the following form:

$$\dot{x}_b = S_t . A_{front} . Q_{fuel} = S_t . A_{front} . \frac{m_{fuel} E_{fuel}}{V_{cyl}}, \tag{5}$$

being A_{front} the spherical front surface area, m_{fuel} the total mass of fuel at ignition, E_{fuel} the specific heat of fuel and V_{cyl} the current combustion chamber volume.

Due to fluid properties notary changes with temperature increments, suitable correlations were introduced to estimates the constant pressure heat capacity (C_p), the thermal conductivity (l) and the dynamic viscosity (m).

As previously mentioned, cold dynamic simulations were performed applying constant conditions for inlet and outlet boundaries. However, for hot dynamic simulations constant conditions are far to be realistic, due to combustion induces dynamic temperature and pressure waves inside ducts. Moreover, CFD simulations consider just a fraction of the overall engine, so the influence of the other cylinders has to be considered. For all these reasons were achieved 0/1-dimensional (0/1-D) simulations of the overall engine, using an engine simulator developed in CIMEC (engine simulator web page). Then, from 0/1-D results were extracted the state variables (pressure, temperature and turbulence) needed to feed the hot dynamic boundary conditions to CFD simulations.

3. RESULTS AND DISCUSSION

In this section first the numerical and experimental data obtained during static tests are introduced. Results showing the reliability of CFD computation to predict the behavior of in-cylinder complex flows are included. Then dynamic simulation results, flow patterns and averaged quantities are shown in order to conclude about the differences between static and dynamic test conditions.

3.1.1 Static flow tests

Figure 4 shows numerical and experimental results of discharge coefficients for the intake (left side) and exhaust (right side) systems. As it can be see, an acceptable concordance is obtained between CFD and experimental results. Differences are bigger at the mean lift range and the averaged relative errors are closer to 6.5%, while maximum relative errors are around 10%. As noted, both the discharge (C_D) and the flow (C_f) coefficients are drawn, due to the fact that the former considers the valve curtain area, it has more sensibility at low valve lifts, while the later uses the constant cross section area of the valve seat, reflecting the behavior of the overall port for high valve lifts (Xu, 2001).

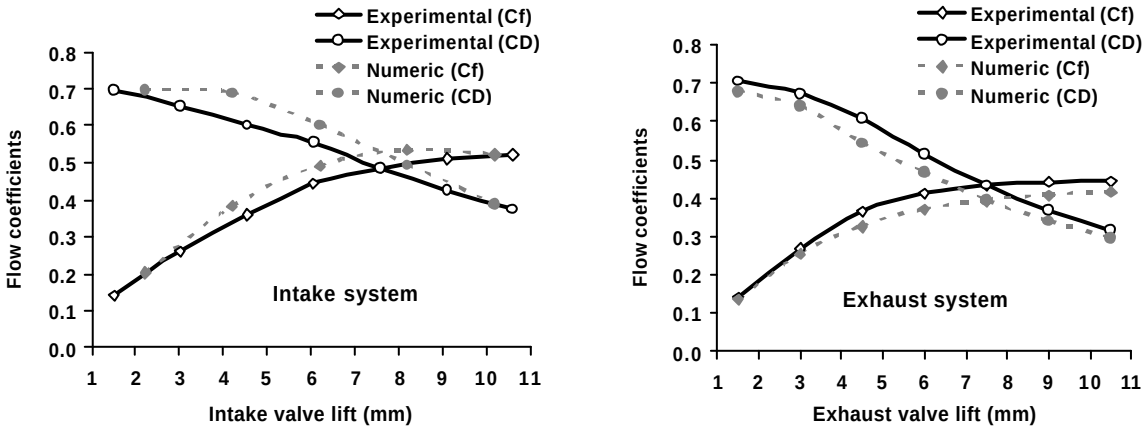

Figure 4: Discharge coefficients (C_D and C_f) for intake (left) and exhaust (right) systems.

By comparing the flow coefficients (C_f) of both ports the exhaust one has a better efficiency at low valve lifts (below 4.5 mm), but the intake system become 17% more efficient when the maximum valve lift is reached. As consigned in table 1, maximum valve lifts are equal to 9 mm and 8.5 mm for the intake and exhaust systems, respectively. This valve timing seem to be appropriate due to the fact that a maximum mass flow increment of 2.5% may be achieved by increasing the intake valve lift from 9.09 mm to 10.6 mm, while for the exhaust system is less than 1%.

3.1.2 Swirl tests

As expected, a 4-valve cylinder engine does not induce meaningful swirl momentum quantities. So, two swirl test strategies were employed to explore the potentiality of the cylinder head to produce swirl. First, one intake valve was kept close while the other was opened (called test 3). Next, both valves were opened but one of them was retarded 1.51 mm with respect to the other (called test 4). Numerical and experimental results are showed in figure 5 for both valve opening configurations. In order to compare numerical and experimental results, the measured angular speed of the honey comb was converted to angular momentum (kg/ms) by applying the assumption that the flow rotates around the cylinder axis as a rigid solid. That means, fluid tangential velocity (V_t) for any in-cylinder point is the product of the measured angular velocity (ω) and the distance (r) from this point to the cylinder axis. Then, the swirl momentum is obtained by the following integration:

$$M_s = \int_{vol} r.V_t.r.dV = \int_0^R 2.p.r.l.r.r.w.r.dr = 2.p.l.r.w \int_0^R r^3.dr = p.l.r.w\frac{R^4}{2}, \qquad (6)$$

being R the cylinder radius, r the fluid density and l the cylinder height (100 mm).

As shown in the figure 5, correlation between numerical and experimental data is good, although the differences on mass flow rate grow for the second valve opening configuration (test 4). Looking at the left graphic in figure 5, the swirl generation is fairly linear when only one valve is opening (test 3), even while, for high lifts the mass flow keeps nearly constant. As was mentioned, this characteristic behavior does not be related to the overall entering mass flow but by changes on the flow direction through the valve while lift is increased. Analyzing the second valve opening configuration (test 4), it is notary how the delay between valves induces small swirl values for medium valve lifts, but once lifts overcomes the asymptotic mass flow rate zone (after 7.57 mm valve lift) then the mass flow through both intake valves become nearly similar and swirl diminishes. Grimaldi et al. (2005) found similar results by experimental static tests, while Mahrous et al. (2007) by dynamic simulations found that in order to induce significant swirl quantities is necessary to have differences upper than 100% between both valve lifts.

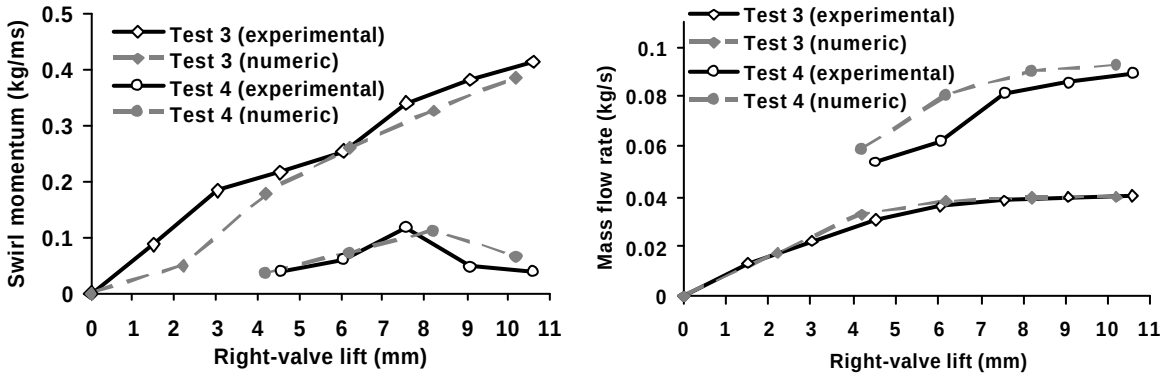

Figure 5: Numerical and experimental results from swirl tests. *Left:* swirl momentum. *Right:* mass flow rate.

Figure 6 shows the mass flow rate distribution around the valve curtain of one valve for the maximum valve lift analyzed (10.6 mm). As noted, when only one valve is opened (test 3) flow distribution is oriented towards the 2-3 direction, influenced by the intake duct. On the other hand, when both valves are equally opened the flow is oriented towards the central zone

between valves. This effect has been also reported by other researchers (Mattarelli, 2000; Grimaldi et al., 2004).

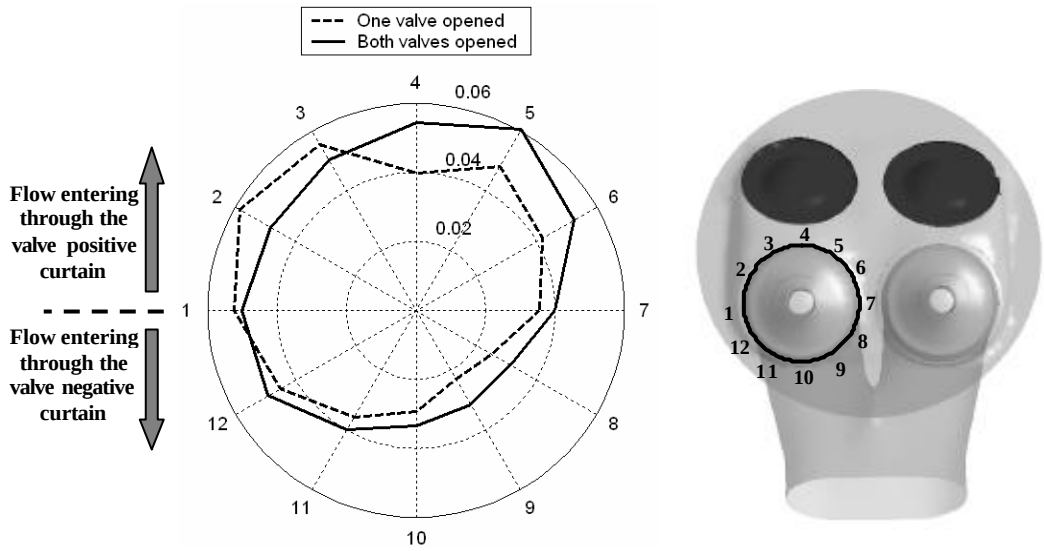

Figure 6: Mass flow rate distribution around the valve curtain by opening both valves (solid line) and only one of them (dashed line).

It is important to mention that the swirl test configuration (incorporating the swirl meter) did not introduce noticeable pressure drops. By comparing the results obtained with the swirl meter (swirl test configuration) and without it (standard flow tests) the mass flow rate loss for the maximum valve lift was only 0.4%. As regard tumble configuration, the tumble bench introduces more pressure drop, so the mass flow rate for the maximum lift is reduced in 7%

3.1.3 Tumble tests

In section 2.1.1 it was displayed the tumble-bench configuration adopted based on a previous CFD study (Ramajo, 2008). In the current section the numerical and experimental results obtained by using this device are presented. Also in this case, the angular speed from the swirl meter results was converted to angular momentum by applying the rigid-solid assumption. Figure 7 shows data obtained by evaluating the tumble at two positions along the lateral duct of the tumble bench (see positions P_2 and P_4 in figure 1). Besides, the in-cylinder tumble numerical results were also drawn in the graphics. Good agreement was found for low valve lifts data at both locations (P_2 and P_4). Moreover, tumble drop is well predicted by CFD at medium valve lifts, however for the position P_2 the tumble is significantly overestimated, being the maximum relative error closer to 61% for 7.57 mm valve lift, being the averaged relative error 25%. As regards position P_4, the maximum relative error reaches 32% (for the same lift), but the average value grows to 32%. As noted discrepancies between numerical and experimental results are noticeable, but similar studies performed for others researchers have found errors even worse, up to 100% (Grimaldi et al, 2003; 2004). By comparing the experimental results at both measurement positions (P_2 and P_4), they show similar behavior, indicating that momentum losses are fairly linear along the lateral duct. The momentum loss between P_2 and P_4 is around 14% for the maximum valve lift (10.6 mm). Similar values are reported with another tumble bench configurations. From numerical simulations it can be seen that the tumble-drop effect at medium valve lifts also takes place inside the cylinder, but it is smoother.

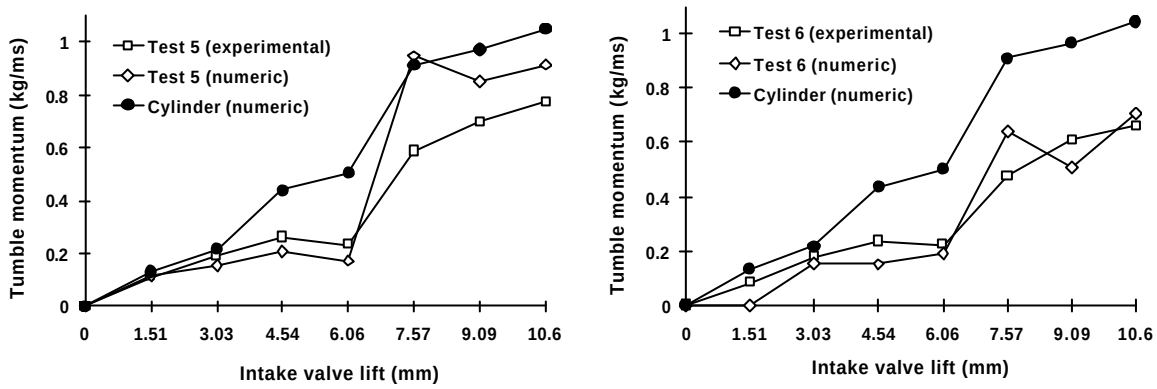

Figure 7: Numerical and experimental results from tumble tests. *Left:* swirl momentum. *Right:* mass flow.

By tracing a right line connecting the first and the last point in each curve it is easy to note that tumble generation is almost linearly proportional to valve lifts, except for the medium valve lift range, where tumble-drop effect occurs. Significant differences appear in the velocity patterns below valves, as can be seen in figure 8. The flow pattern at 3.03 mm is characterized by four small vortexes, one at each side of the intake valves. Vortexes spin allowing flow discharges all around valves and especially through the inter-valve zone. For medium valve lifts (from 4.54 mm to 7.57 mm) one big vortex is placed below each valve. As shown, both structures have the same rotating sense, so while the left vortex favors the flow entrance through the mean valve zone, the other vortex opposes to it. Finally, when valve lifts reach 7.57 mm flow pattern become similar to that found at low lifts. It indicates that for low and high valve lifts flow behavior is similar and tumble increases as long as lift does.

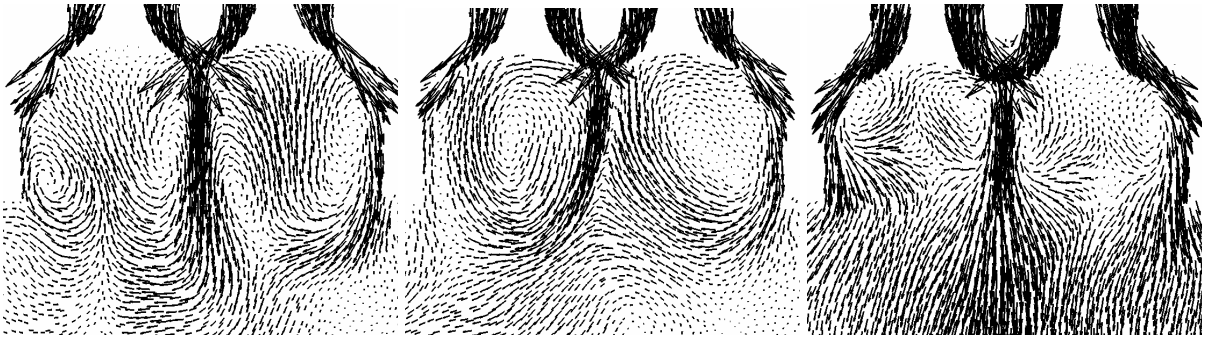

Figure 8: Velocity patterns below intake valves for two valve lift. *Left:* 3.03 mm. *Center:* 4.54 mm. *Right:* 7.57 mm.

The mass flow rate distributions around the valve curtains are shown in figure 9. As noted for low and medium valve lifts (less than 6.06 mm) a significant fraction of the flow enters into the cylinder following the direction gives by the intake port (see a detail of engine geometry at right) and through 8-9 and 11-12 directions for left and right valves respectively. But while valve lift increases the flow distribution strongly changes and the flow is progressively oriented towards the central zone between the intake valves.

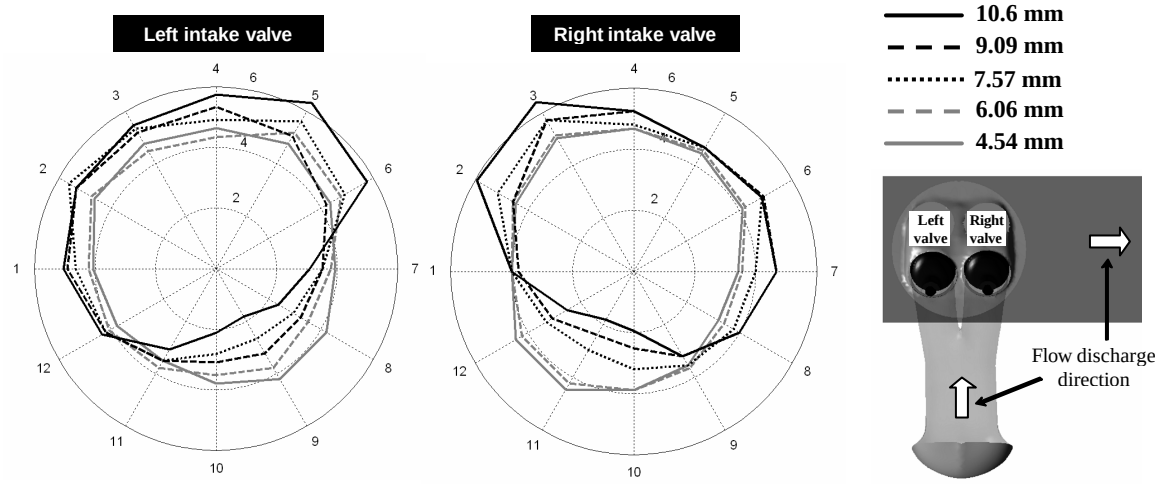

Figure 9. Mass flow rate distribution around the valve curtains by opening both valves.

In figure 10 the results of 4 strategies to induce momentum (swirl or tumble) by using different valve opening strategies are drawn. As it is displayed full tumble configuration (corresponding to equal valve opening) seen to be the most effective form to induce in-cylinder momentum. Although the strategy of introducing a small lift retard (of 1.51 mm) smoothes the tumble generation curve, it also produces a significant mass flow rate loss at low and medium valve lifts. On the other and, when only one valve is opened (full swirl), the momentum generation is less than a half of the full tumble momentum and the mass flow rate reduces more than 50%.

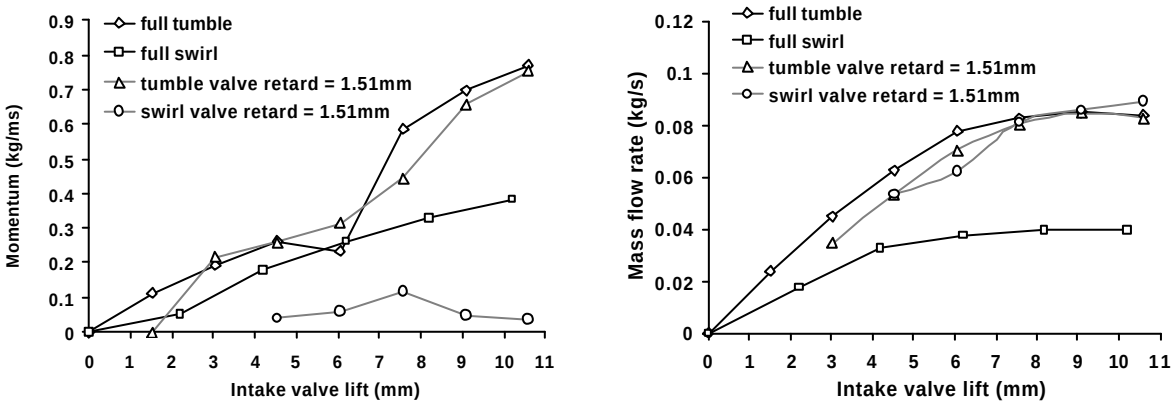

Figure 10: 4 strategies to generate in-cylinder angular momentum (swirl or tumble). *Left:* angular momentum values. *Right:* mass flow rates.

Of course, the swirl generation and mass flow rate for a 2-valve engine would be always greater than that obtained by open only one intake valve of a 4-valve engine. The aim of this comparative analysis is to know the intensity of the different flow vortex structures (tumble and swirl) that may be potentially induced by using variable valve lift (VVL) configurations. In this sense, as shown un several previous papers (Wilson et al., 1993; Geiger et al., 1999; Li et al., 2001; Grimaldi et al., 2004; 2005), static tests are the first step to develop valve opening strategies for controlling the in-cylinder flow motion.

Any valve opening configuration that improves tumble or swirl generation will impact negatively over the engine volumetric efficiency. On the other hand, Ramajo (2008) numerically studied the effect of introducing variable-position flow deflectors inside the intake

port of this engine, obtaining increments on tumble of 18% with mass flow rate losses closer to 10%. As regards swirl generation, incorporating a flow deflector allowed to improve swirl quantities similar to that obtained by keep one valve closed, but introducing an additional mass of 46%.

3.2 Cold dynamic simulations

As was mentioned, the engine behavior for three engine speeds (1500 rpm, 3000 rpm and 4500 rpm) was tested by CFD, covering almost the whole engine work regimen. As showed in figure 3 (section 2.2.3), only one cylinder of the overall engine geometry was modeled.

Simulations started from atmospheric conditions over a quiescent flow but stationary conditions were quickly obtained. Figure 11 shows at top the evolution of the in-cylinder mass flow rate and pressure during 4 engine cycles, obtained at 1500 rpm. Moreover, at the bottom the turbulent kinetic energy (k) and the tumble momentum (M_T) are drawn.

Certain in-cylinder quantities like in-cylinder pressure, temperature or cumulative mass (the last two not included in figure 11) have an insignificant variation along engine cycles. Others like turbulent kinetic energy or tumble momentum display major differences. But from results, it is possible to conclude that since the third cycle the solution does not change notoriously and the state at the beginning and at the end of the cycle is fairly similar. The fast convergence of results could be probably slower for multi-cylinder engines, in which each cylinder induces pressure waves in manifolds at different times, so the stationary conditions on ducts and plenums are delayed for the interaction of all cylinders.

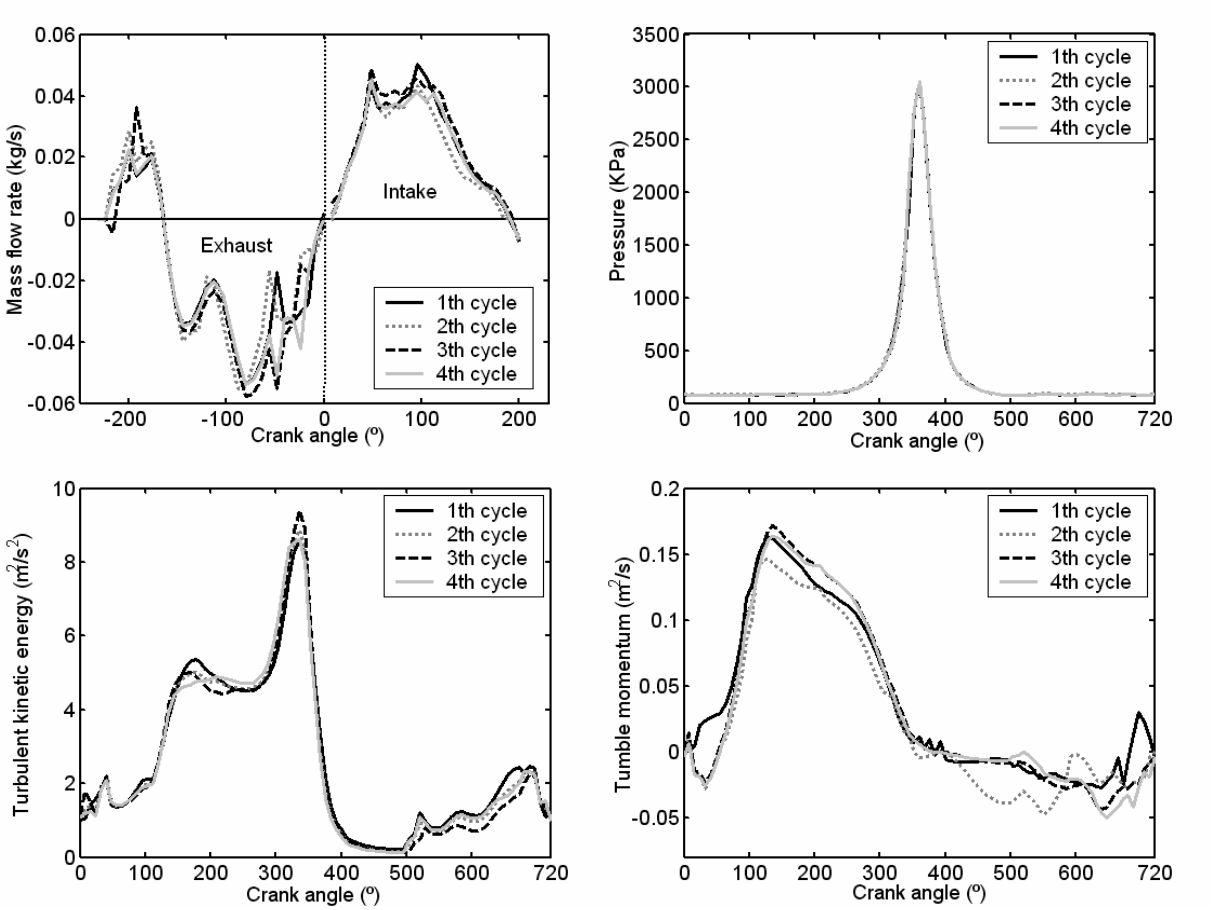

Figure 11: Evolution of some relevant quantities along 4 engine cycles. *Upper left:* mass flow rate. *Upper right:* pressure. *Bottom left:* turbulent kinetic energy. *Bottom right:* tumble momentum.

3.2.1 Flow patterns

Figure 12 shows the evolution of the velocity field during intake and compression strokes over a plane cutting one intake valve. As noted, the vortex dynamics is very complex over that plane. Several structures are created and destroyed while admission and compression process occurs. In pictures have been identified the main structures taking into account their rotation sense, using circles for clockwise sense (positive tumble) and squares for counter clockwise (negative tumble). Moreover, structures are also classified attending to their size (solid for big and hollow for small structures).

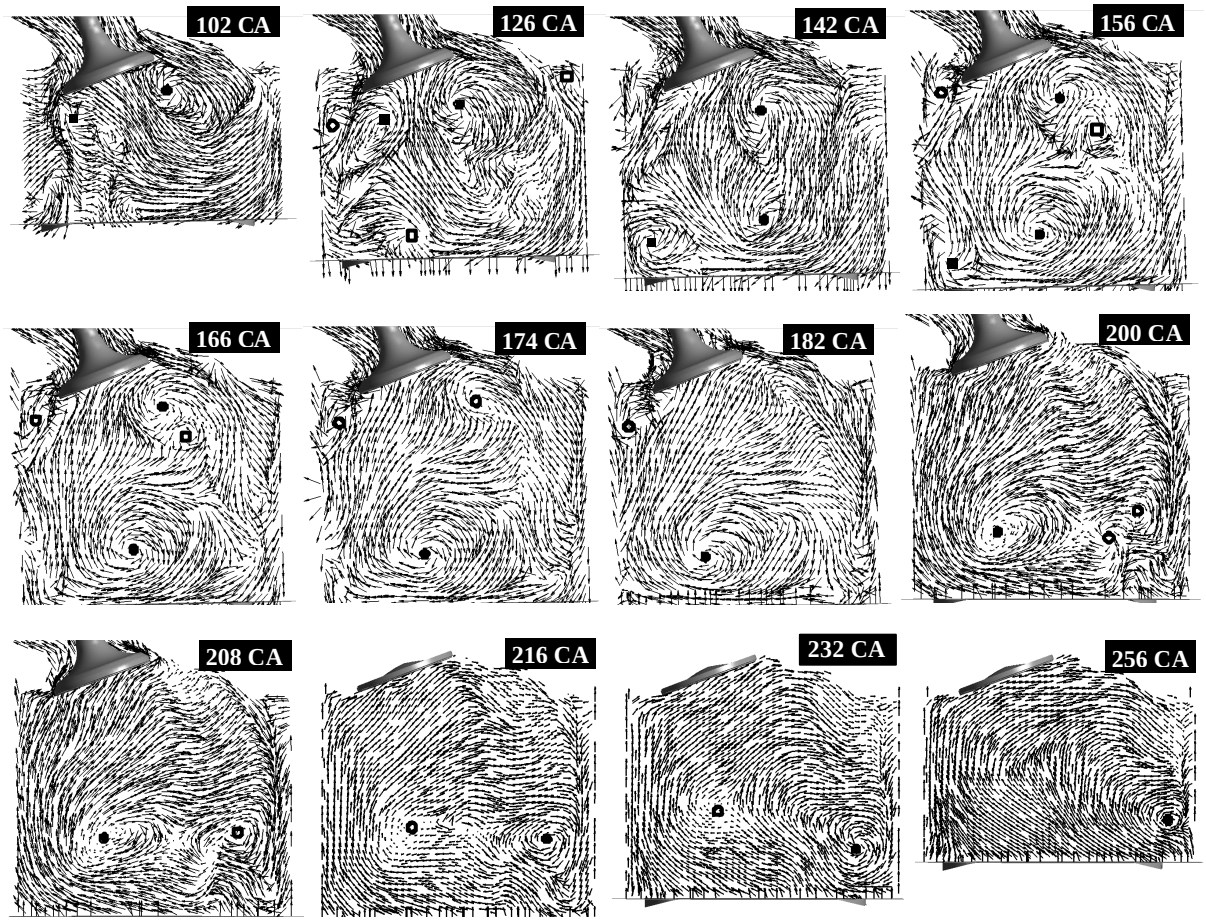

Figure 12: Evolution of flow during the intake and compression strokes over a plane cutting one intake valve.

The flow over planes perpendicular to the cylinder axis is fairly similar for the three engine speeds analyzed. In figure 13 are shown the flow patterns over two planes located at 10 mm and 30 mm below the top dead center (TDC) at the instant of maximum valve lift (102 CA). For planes *A* and *B* it is able to identify 11 (plane *A*) and 8 (plane *B*) structures that are present for the three engine speeds. That means, even though in-cylinder flow is strongly complex, engine speed seen to have a small effect over flow characteristics, although as expected, velocity magnitude is increased. Flow pattern similitude is partially lost when combustion is considered due to the localized increment of the in-cylinder pressure and due to its major influence on pressure differences and acoustic waves in ducts and plenums than cold engine simulations (Ramajo, 2008).

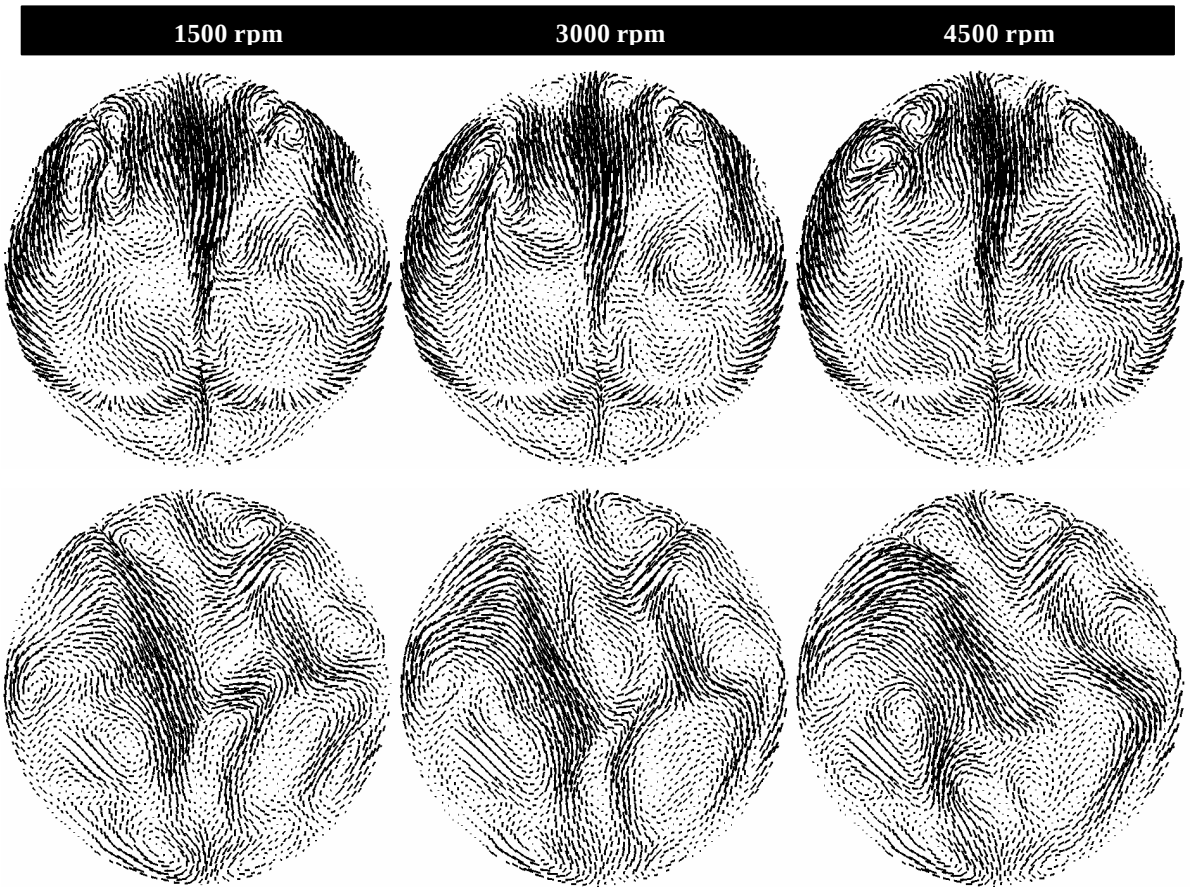

Figure 13: Flow patterns over two planes located at 10 mm (upper figures) and 30 mm (bottom figures) below the top dead center (102 CA).

3.2.1 Averaged quantities

Figure 14 shows the in-cylinder spatial average of tumble momentum (M_T) and turbulent kinetic energy (k) from the last engine cycle and for three engine speeds. As for tumble momentum, it is negative until the firsts 50 CA. Then it is follow by a faster tumble increment, reaching the maximum around 150 CA. Subsequently, the tumble evolution is nearly linear from 150 CA to 280 CA, and finally a quickly degradation occurs at the end of the compression stroke. Tumble keeps null during the expansion and the first stage of exhaust strokes, but flow evacuation at the end of cycle (630 to 720 CA) induces significant negative tumble momentum that, in part, explain the tumble generation delay at the beginning of the next cycle. As showed in figure 11, this effect is not appreciated for the first engine cycle.

The production of turbulent kinetic energy is mainly due to two effects; on the one hand, because of the frictional efforts and flow detachment around valves along with large strain gradients during the intake and exhaust stages, and on the other hand, for the tumble degradation along the compression stroke. The first effect produces a local maximum of k around 170 CA. The second one leads to a significant increment of k around 360 CA (TDC), being it the maximum turbulent kinetic energy of the whole engine cycle. Turbulent kinetic energy keeps almost zero during the expansion stroke and the first stages of the exhaust one. Finally, little turbulence is produced during the gas evacuation. As shown in figure 14, the creation of macro-vortex structures guarantees the conservation of a high portion of the kinetic energy of the inlet gases until the end of compression. Then, the energy transfer from the mean flow to the smallest turbulent structures (micro eddies) induces a maximum of turbulence close

to the spark ignition instant, increasing the mass burn rate and improving the overall combustion (Jeon et al., 1998; Aleiferis et al, 2004; Li et al., 2001; Mariani and Cavalletti, 2004; Ramajo, 2008). By comparing the results obtained from the dynamic simulation of the Fiat Torque engine with respect to the corresponding to two 4-valve academic-geometry engines obtained from a previous work (Ramajo et al., 2007), it is possible to conclude that the Fiat Torque cylinder head has a low to medium capacity to produce tumble, but at the same time, it shows a low tumble dissipation rate along the compression stroke, allowing the noticeable turbulent enhancement during the ignition time.

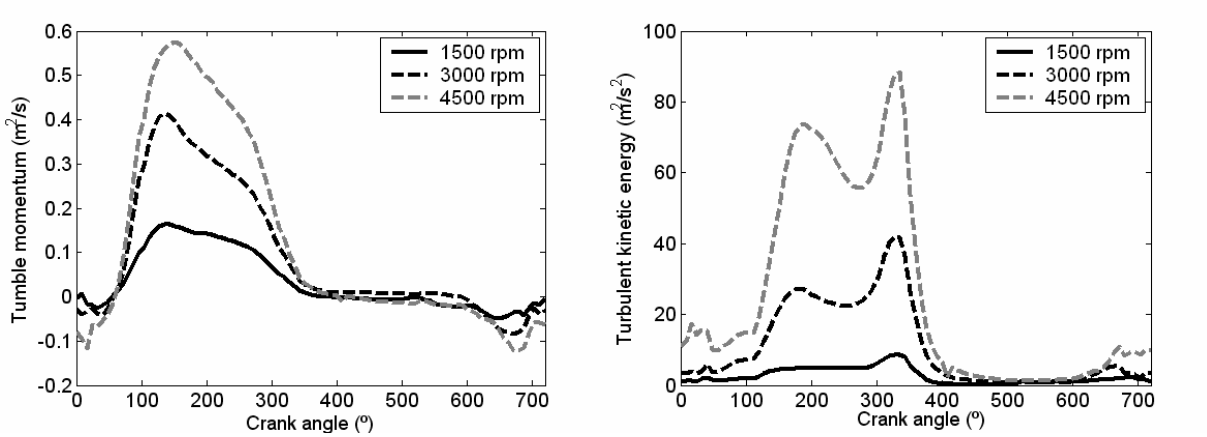

Figure 14: Tumble momentum (*left*) and turbulent kinetic energy (*right*) for three engine speeds.

Table 2 consigns the tumble momentum and turbulent kinetic energy results for three instants; the maximum peak (the corresponding crank angle is also included), at 342 CA (closer to the instant when spark plug takes place) and at 360 CA (TDC). The mass flow rate for the maximum valve lift is also displayed.

Engine speed	M_T **(m²/s)**			$\dot{m}$ **(kg/s)**	k **(m²/s²)**		
	Max.	**342 CA**	**360 CA**	**102 CA**	**Max.**	**342 CA**	**360 CA**
1500	0.164-136CA	0.014	0.005	0.0373	8.6-336 CA	8.0	4.0
3000	0.415-136CA	0.036	0.02	0.0792	41.9-328 CA	36.1	18.6
4500	0.575-152CA	0.05	0.021	0.1207	88.5-336 CA	79.1	37.2

Table 2: Tumble momentum (M_T), turbulent kinetic energy (k) and mass flow rate ($\dot{m}$) for several instants along the intake and compression stroke.

Table 3 is useful to clarify the influence of engine speed on M_T, k and $\dot{m}$. For low engine speeds (increment from 1500 to 3000 rpm), all quantities grow more than the engine speed increment (which is of 100%). Tumble momentum increases between 150% and 300% while turbulence grows more than 350%. However, when the engine speed up to 4500 rpm (increment from 3000 to 4500 rpm) then M_T is scarcely incremented and at 360 CA the effect of engine speed over tumble intensity is negligible. On the other hand, the turbulent kinetic energy is increased in a similar way to engine speed, so k increments must not be related to tumble degradation but to flow strain efforts.

Engine speed increments	Percentage increments (%)							
	rpm	M_T			$\dot{m}$	k		
		Max.	342 CA	360 CA	102 CA	Max.	342 CA	360 CA
1500 a 3000	100	153	157	300	112	387	350	365
3000 a 4500	100	38	39	5	53	111	119	100
1500 a 4500	200	250	257	320	224	929	889	830

Table 3: Increments on tumble momentum (M_T) and turbulent kinetic energy (k) and mass flow rate ($\dot{m}$) for several instants along the intake and compression stroke while engine speed increases.

3.3. Static and cold dynamic flow test comparison

It is interesting to compare the mass flow distribution around one valve curtain for different valve lifts and for static and dynamic tests. Static results used for comparison in this section correspond to the static tumble test. In figure 15 the mass flow distributions from dynamic tests for valve lifts of 4 mm, 6 mm, 8 mm and 9 mm are drawn, separating the events of valve opening or closing. Also, in the same pictures the distributions corresponding to static tests are included. Of course, for the later there is not differences about opening and closing. As quickly noted, flow behavior is fairly similar during opening along the analyzed engine speeds, but it completely changes during closing. Static distribution seems to be similar to dynamic one while valve is opening, but differences become significant when the maximum lift is reached. The canalization effect of flow towards the zone between valves is more relevant for the dynamic cases, and for the maximum valve lift valve the percentage of mass flow entering through the negative valve curtain (from 7 to 1) diminishes respect to the static case. The significant non homogeneous flow distribution found for dynamic cases enhances tumble generation at high valve lifts over the static estimations. The mass flow fraction entering through the negative valve curtain reduces even more during valve closing, improving more the capacity to generate tumble of the engine.

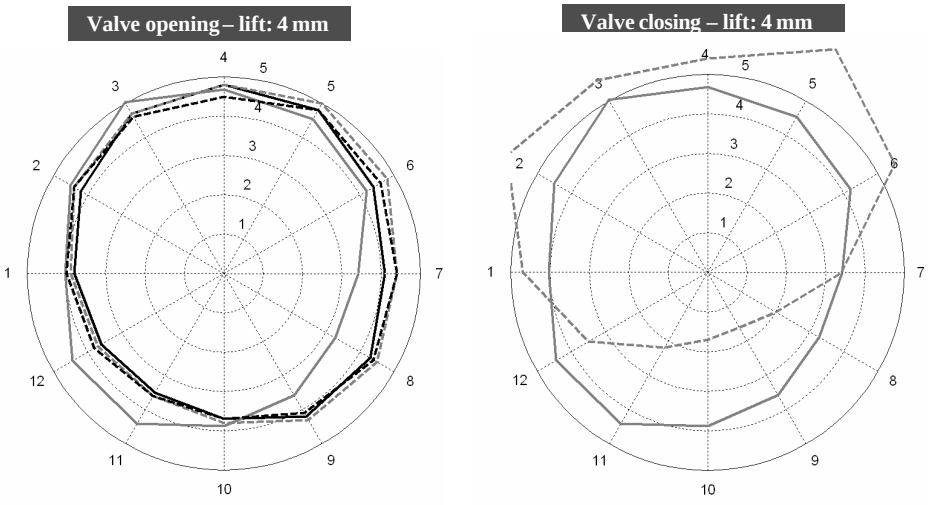

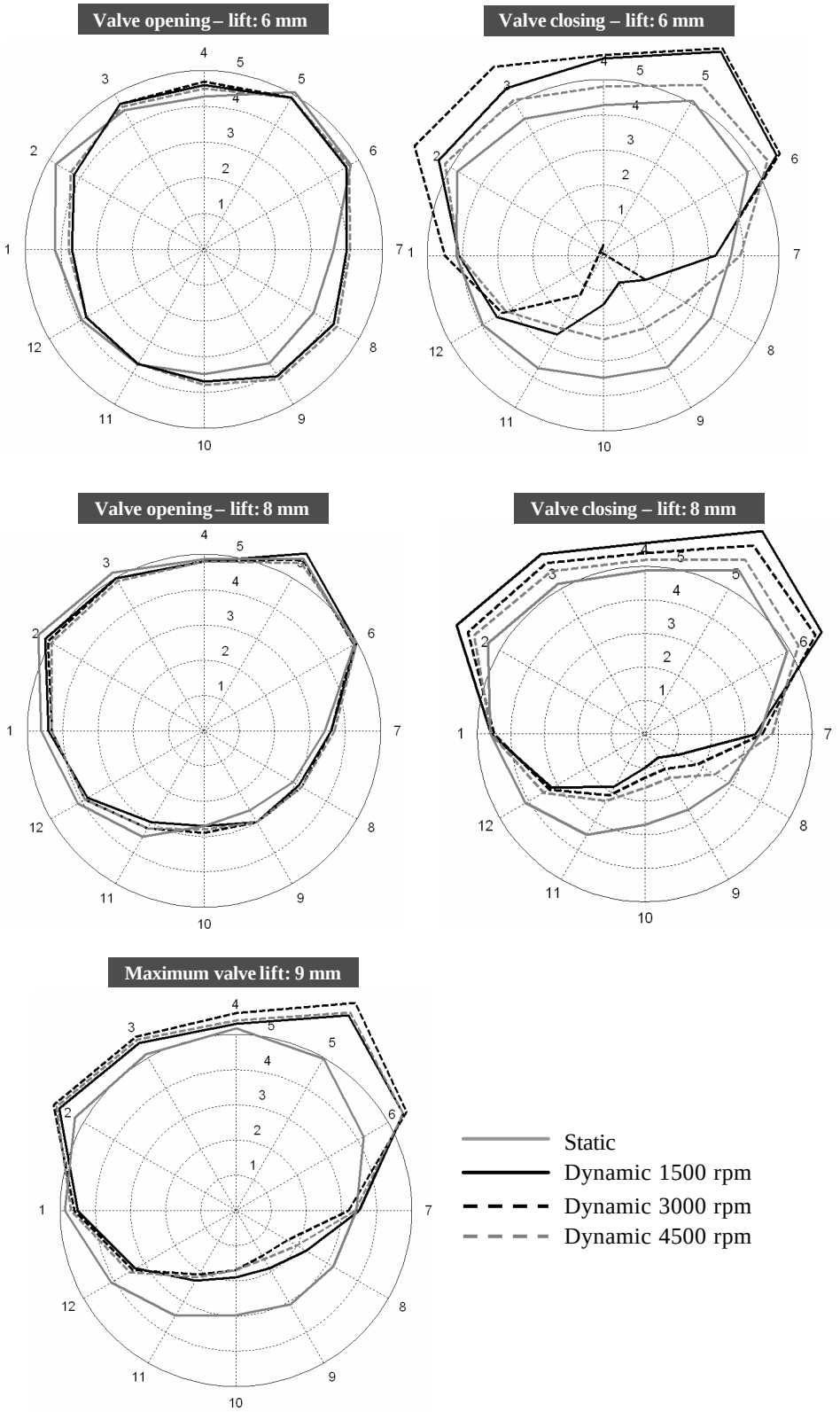

Figure 15: Mass flow distribution around one valve curtain for several valve lifts and static and dynamic situations.

In figure 16 the flow patterns over a plane cutting the intake valves for the maximum valve lift (9 mm) are displayed. As noted in the first picture at top (static case), vortex structures

appears at both sides of each valve and very close to the valve head. Dynamic results are similar among them but differ considerably from the static one. Nevertheless, also it can be defined small vortex structures near to the valve heads. Configuration differences between static and dynamic (real) tests become significant. For static tests, the piston is not considered and for the tumble bench employed the discharge enclosure is big while for the dynamic case the piston head is near valves (at 102 CA the piston has gone down a bit more than a half of stroke), so the combustion chamber is small and tumble vortex rotation obstructs the flow discharge through the negative curtain (from 7 to 1 in figure 15). This effect can be noted by looking the graphics corresponding to maximum valve lift and valve closing in figure 15.

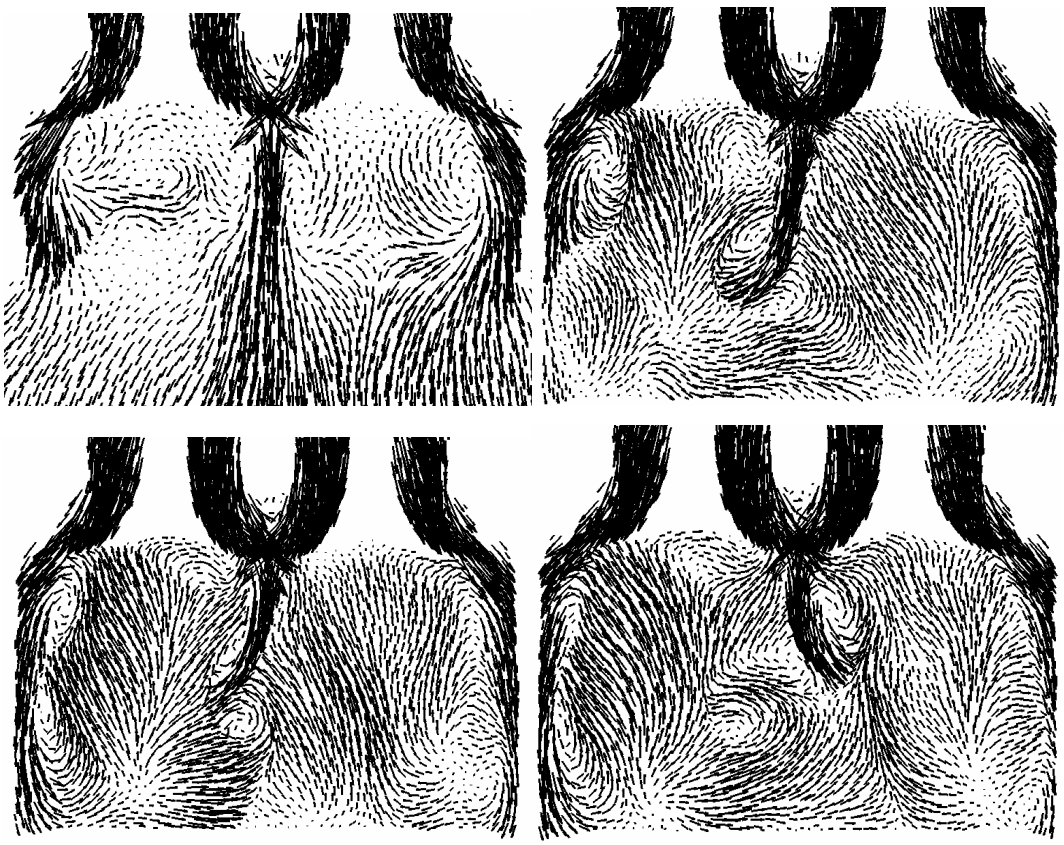

Figure 16: Velocity patterns over a plane cutting the intake valves for the maximum valve lift and static and dynamic tests.

Figure 17 at left shows the tumble generation along the intake process as a function of the valve lift. As noted, positive tumble starts producing since 7 mm valve lift, even though, from figure 18 the mass flow rate before 7 mm valve lift is significant. As was previously mentioned, negative tumble during the first stage of intake process is related to the end of exhaust process. The vertiginous increment of tumble since 7 mm can be explained by the change on mass flow distribution around valve curtains (showed in figure 15), since until 7 mm distributions are almost homogeneous but from 7 mm flow start to turn toward the curtain positive zone. It is curious that for the three dynamic cases the around 70% of maximum tumble is generated at the maximum valve lift. Once maximum tumble is reached (around 8 mm valve lift while valves are closing), tumble decreases almost linearly while valves close. Thereafter, tumble continues diminishing linearly until the last stage of the compression stroke, as shown in figure 14.

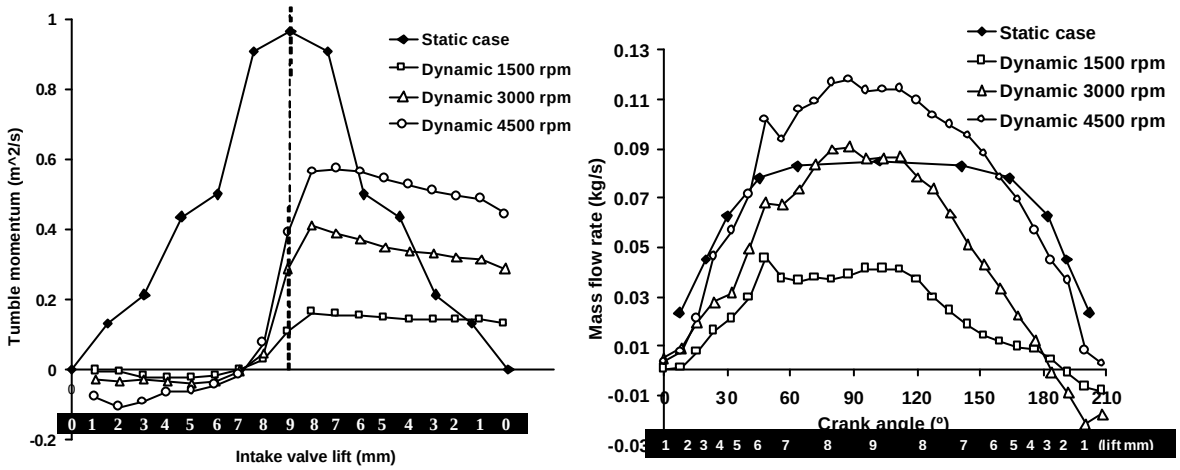

Figure 17: Tumble momentum as a function of valve lift for static and dynamic tests (*Left*) and mass flow rate along intake process as a function of valve lift (*Right*).

In figure 17 at right it can be seen in the same graphic the mass flow rate obtained by static and dynamic tests. It is difficult to conclude about the relationship between static and dynamic tests because the first are made under constant pressure drops and flow is completely developed before measurement (stationary conditions). While for the other, in-cylinder pressure depends on piston cinematic and stationary conditions are farther to be reached. If the static curve is scaled in such a way the mass flow rate at maximum valve lift coincides with each one of the dynamic results (similar to that occurs with the dynamic case at 3000 rpm), then an overestimation of the mass flow rate predicted by static tests is found. Differences are bigger for valve closing than for valve opening, which is consistent with the behavior found by drawing the mass flow distributions in figure 15.

3.4 Hot dynamic simulations

As explained before, dynamic boundary conditions extracted from 0/1-dimensional simulation and a phenomenological combustion model were implemented for perform the hot dynamic simulations. Results for the same three engine speed (1500, 3000 y 4500 rpm) were achieved and the most significant differences respect to cold dynamic results are detailed below.

3.4.1 Averaged quantities

As for mass flow, the main differences between cold and hot simulations are found at the beginning and at the end of the cycle, and they are related with the fast flow discharge that occurs when exhaust valves open. As shown in figure 18, during cold conditions, the flow is pushing or sucking because of piston motion, but when combustion is incorporated, the in-cylinder pressure and the pressure waves it ducts define the flow dynamics. As noted, intake process is fairly similar for cold and hot simulations. But notary differences appears when exhaust valves open and the maximum mass flow rates for the cold case take place close to the maximum exhaust-valve lift while for the hot case they occur immediately after valves start opening.

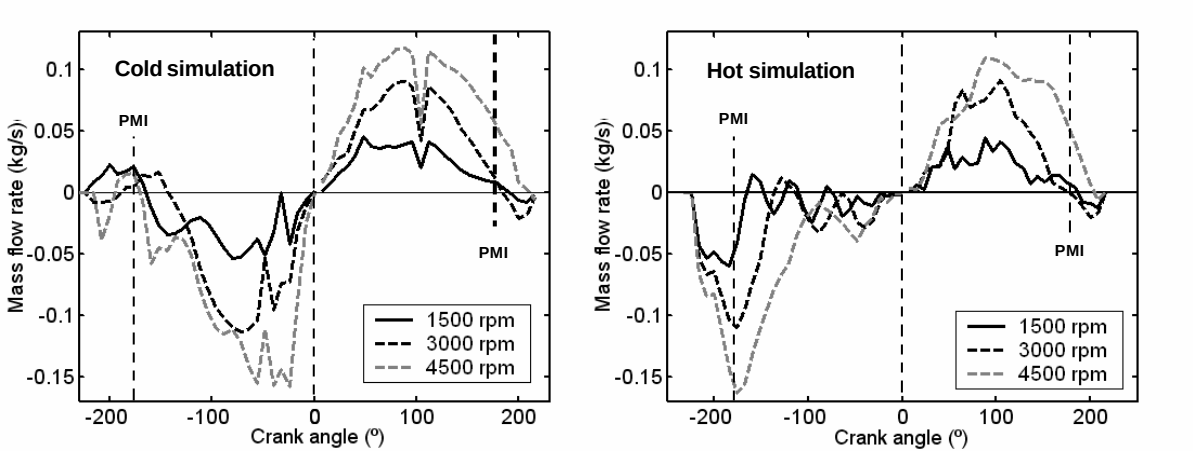

Figure 18: Mass flow rate for cold (*left*) and hot (*right*) dynamic simulations.

Comparing figures 19 and 14, tumble momentum is similar for hot and cold simulations. Maximum tumble be increased for the hot case (20% and 18% for 1500 and 3000 rpm, but just 4% for 4500 rpm), although the overall tumble evolution is nearly the same. More significant oscillations of tumble are found at the end of the cycle, due to the mass flow rate oscillations (showed in figure 18).

As regards the turbulent kinetic energy (k), differences between cold and hot results become notorious while engine speed increases. Turbulent kinetic energy is bigger for hot simulations than the cold ones. Moreover, for hot results the first peak (found during the intake process) takes more relevance and for 4500 rpm it became dominant over the second peak (related to tumble degradation).

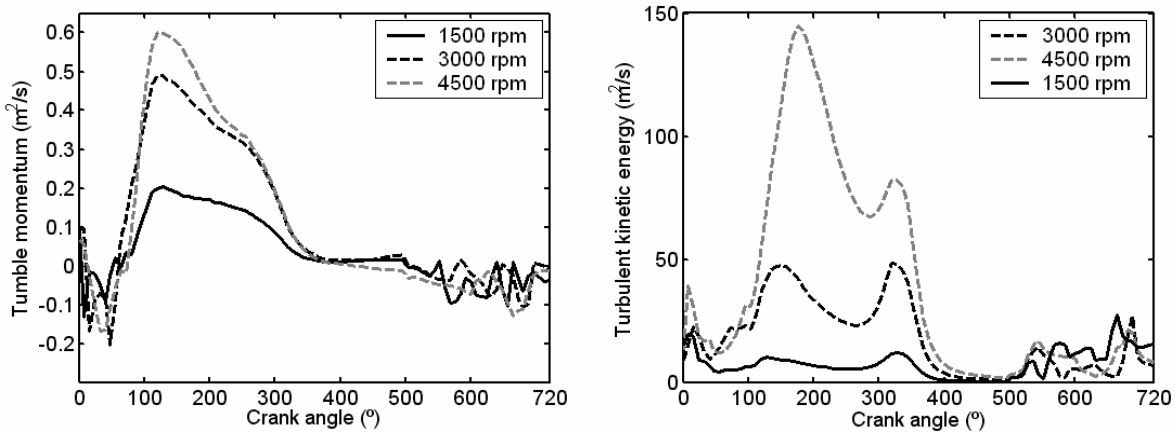

Figure 19: Tumble momentum (*left*) and turbulent kinetic energy (*right*) for three engine speeds.

The table 4 consigns the percentage increments caused by combustion. As noted, the effect of combustion over tumble reduces while engine speed increases, although tumble is always growing. As for turbulence, a similar effect is appreciated.

	Percentage increments by introducing combustion (%)						
	M_z			$\dot{m}$	k		
	Max.	342 CA	360 CA	102 CA	Max.	342 CA	360 CA
1500	22	71	190	2	37	33	26
3000	18	39	40	15	16	17	19
4500	4	0	5	-12	64	4	3

Table 4: Percentage increments on tumble momentum (M_T) and turbulent kinetic energy (k) by introducing combustion.

3.4.2 Combustion behavior

Figure 20 at the left displays the evolution of the characteristic variables of the combustion model for 1500 rpm, while at the right are drew the turbulent burning velocity for the three engine speeds. The Front radius is the time integral of the turbulent burning velocity. By analyzing the Front area it is noted that the curve changes when the flame from takes contact with the piston surface (around 355º CA) and with the cylinder surface (around 405º CA). Although the employed combustion model is extremely simple, it allows estimate the influence of tumble and turbulence on combustion performance. As noted in figure 20 at right, ignition advance is increased along with the engine speed, but although the burning velocity grows with engine speed, the overall combustion period is extended, as can be seen in table 5.

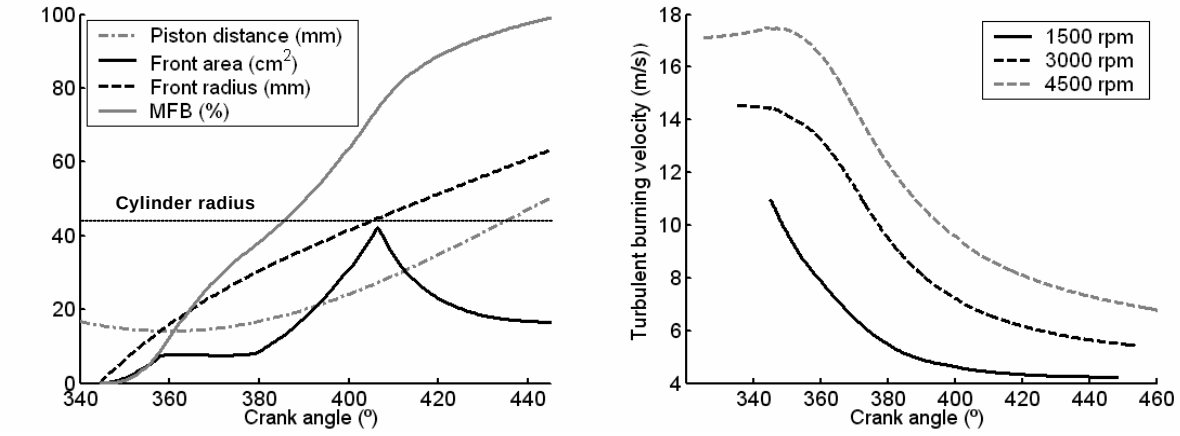

Figure 20. Combustion variables for 1500 rpm(*left*) and turbulent burning velocity (*right*) for three engine speeds.

Engine speed	j_{ig} (CA)	Dj_{comb} (CA)	Dt_{comb} (ms)	$\overline{u'}$ (m/s)	$\overline{S_t}$ (m/s)
1500	344	101	11.22	1.97	4.578
3000	335	120	6.66	3.02	9.076
4500	325	133	4.93	4.1	11.786

Table 5: Ignition time (j_{ig}), combustion duration in CA (Dj_{comb}), combustion duration in ms (Dt_{comb}), averaged turbulent intensity ($\overline{u'}$) and averaged turbulent burning velocity ($\overline{S_t}$).

4. CONCLUSIONS

In this work were performed numerical and experimental cold tests over a commercial 4-valve spark ignition engine. Static tests allow know same mean-flow characteristics of the cylinder head like the mass flow discharge coefficients and the capacity of produce angular momentum (tumble and swirl). From numerical and experimental results it was able to establish the reliability of CFD techniques to study the complex in-cylinder flows that take place. About these could be arrived to the following conclusions:

- experimental static tests quickly give information about the characteristics of the cylinder heads. They have sensibility to compare geometrical modifications over the engine, improving discharge coefficients or promoting tumble and swirl generation
- CFD technique gives acceptable results for complex flows so it can be employed to study in depth the in-cylinder flow patterns. CFD allowed study the tumble-generation drop at medium valve lifts, also detected by experimental tests. Moreover, numerical results displayed that this phenomenon can be explained by changes in the vortex structures bellow valves
- valve opening strategies, like retard or keep closed one of both valves, seem to be a useful methodology for controlling in-cylinder flow structures, but swirl generation in 4-valve engines requires high retards and swirl production go down at high valve lifts
- experimental and numerical results showed the existence of a cooperative effect when both valves are opened, improving the discharge flow coefficients.

Then, cold dynamic simulations were achieved and comparison with static results allowed arise to the following conclusions:

- in-cylinder stationary conditions are quickly reached and two or three thermodynamic cycles are enough to obtain acceptable results. Probably it is not enough for pluri-cylinders engines, and more even for hot engine simulations
- for the analyzed engine, tumble motion dominates over the other two angular components and the same behavior is found for the whole engine speed. Tumble starts growing after 50 CA and its maximum is located around 144 CA. Then a fast degradation takes place between 280 and 360 CA, destroying all the rotational motion. Finally, after 630 CA the exhaust gases induce significant negative tumble
- tumble generation occurs after 8 mm intake-valve lift is reached (before that tumble is negative). The 70% of the maximum tumble is get at the maximum valve lift (9 mm), and the peak takes place as soon as valves start closing (at 8 mm). The abrupt tumble increment nearby maximum valve lift is a consequence of changes on the mass flow distribution of the entering flow around intake valves
- turbulent kinetic energy shows two peaks; the first one during the intake process (around 150 CA), and the main one because of the tumble degradation at the end of the compression stroke
- the flow structures over cross transversal planes show notary similitude for the three engine speed analyzed
- tumble-vortex dynamic is more complex over the planes cutting the intake valves than over the mean cylinder plane. There is creation and destruction of structures along all intake period, and at less three main tumble vortexes can be defined for different times
- tumble generation is strongly related with engine speed but relative increments of tumble are more appreciable from 1500 to 3000 rpm than from 3000 to 4500 rpm. A similar behavior is found for the turbulent kinetic energy.

Finally, combustion was toke into account and comparison with cold dynamic simulation led to the following conclusions:

- the combustion model implemented has capacity to predict the evolution of combustion, considering the influence of the turbulence

- to employ dynamic boundary conditions extracted from 0/1-dimensional results allowed to consider the overall engine geometry effects, focusing the analysis on in-cylinder behavior
- differences between cold and hot simulations are clearly visible by drawing the mass flow rate. For the cold case, flow motion is governed by the piston dynamics, while for the other case in-cylinder pressure and pressure waves in ducts control the fluid dynamic
- tumble generation is not strongly affected by combustion. Increments around the 20% are found for 1500 and 3000 rpm, but for 4500 rpm tumble is fairly the same for cold and hot cases
- turbulence is increased substantially during intake period, and for the highest engine speed the maximum generation is due not for tumble degradation but the entrance flow.

5. KNOWLEDGEMENTS

Authors want to thanks to CONICET and ANPCyT (grants PICT Lambda 12-14573/2003, PME 209/2003). Also they are gratefully to Fiat Argentina to donates a Fiat Torque engine to do this work, and finally to thanks Miguel Ramos to help us to perform the experimental tests.

6. REFERENCES

Aleiferis P.G., Taylor A.M.K.P., Ishii K. and Urata Y, The nature of early flame development in a lean-burn stratified-charge spark-ignition engine. *Combustion and Flame*, Vol. 136, pp. 283-302, 2004.

Aquiles Cluster at CIMEC, http://www.cimec.org.ar/aquiles, 2008.

Engine simulator web page: http://wwww.fceia.unr.edu.ar/fceia1/mecanica/Automotores/laboratorio_de_automotores_index.htm

Geiger J., Grigo M., Lang O., Wolters P. and Hupperich P., Direct Injection Gasoline Engines – Combustion and Design, *SAE* paper 199-01-0170, 1999.

Grimaldi C, Battistone M. and Mariani F, Experimental and Numerical Analysis of Charge Motion Characteristics Depending on Intake Valves Actuation Strategies, *SAE* paper 2005-01-0242, 2005.

Grimaldi C, Battistone M. and Uccellani, Dependence of Flow Characteristics of a High Performance S.I. Engine Intake System on Test Pressure and Tumble Generation Conditions- Part 1: Experimental Analysis, *SAE* paper 2004-01-1530, 2004.

Grimaldi C, Battistone M. and Postrioti L, Flow Characterization of a High Performance S.I. Engine Intake System- Part 1: Experimental Analysis, *SAE* paper 2003-01-0623, 2003.

Heywood J.B., Internal Combustion Engines Fundamentals, *Mc Graw Hill*. New York. 1988.

Jeon C., Chang Y., Cho K. B. and Kang K. Y., Effects of Intake Ports on In-Cylinder Flow and Lean Combustion in a 4-Valve Engine, *SAE* paper 981048, 1998.

Mahrous A, Wysznski M, Xu H and Tsolakis A, A CFD Investigation into the Effects of Intake Valves Events on Airflow Characteristics in a Motored 4-Valve Engine Cylinder with Negative Valve Overlapping, *07-NAPLES-74*, 2007.

Mariani F. and Cavalletti M., Dependence of Flow Characteristics of a High Performance S.I. Engine Intake System on Test Pressure and Tumble Generation Conditions – Part 2: Numerical Analysis, *SAE* paper 2004-01-1531, 2004.

Mattarelli E., Comparison between two Combustion Chambers for a Motorcycle Racing Engine, *SAE* paper 2000-01-1894, 2000.

North G. and Santavicca D., The Fractal Nature of Premixed Turbulent Flames, Combustion Science and Technology, Vol. 72, pp. 215-232, 1990.

Li L., Tao J., Wang Y., Su Y. and Xiao M., Effects of Intake Valve Closing Timing on Gasoline Engine Performance and Emissions, *SAE* paper 2001-01-3564, 2001.

López E., Nigro N. and Storti M., Simultaneous untangling and smoothing of moving grids,

International Journal for Numerical Methods in Engineering, in press, 2008.

Ramajo D. Simulación computacional de los procesos fluido-dinámicos en el interior de motores de combustión interna, *PhD thesis*, Universidad Nacional del Litoral, 2008.

Ramajo D, Zanotti A. and Nigro N, Assessment of a zero-dimensional model of tumble in four-valve high performance engine, *Int. J. of Numerical Methods for Heat and Fluid Flow*, vol. 17, no. 8, pp. 770-787 , 2007.

Xu H., Some Critical Technical Issues on the Steady Flow Testing of Cylinder Heads, *SAE* paper 2001-01-1308, 2001.

Tan Z, Reitz R.D, An ignition and combustion model based on the level-set method for spark ignition engine multidimensional modeling, *Combustion and Flame*, Vol. 145, pp. 1-15, 2006.

Williams F., Turbulent Combustion, *SIAM*, Philadelphia, 1985.

Wilson N., Watkins A. and Dopson C., Asymmetric Valve Strategies and Their Effect on Combustion, *SAE* paper 930821, 1993.